Available online at www.sciencedirect.com
ScienceDirect
Journal of Power Sources 159 (2006) 1051–1060
JOURNAL OF POWER SOURCES
www.elsevier.com/locate/jpowsour

An approximate analytical solution to channel flow in a fuel cell with a draft angle

Yongjin Sung *

Hyundai Motor Company, 104 Mabuk-ri, Kuseong-eup, Yongin-si, Kyunggi-do, Korea

Received 17 October 2005; received in revised form 9 December 2005; accepted 12 December 2005
Available online 24 January 2006

Abstract

This paper investigates the channel flow with a suction or injection boundary condition to imitate the reactant flow in fuel cells. A two-dimensional model is proposed for a channel with a trapezoidal cross-section, and systematically analyzed using the perturbation method and the Laplace transform technique. The model predicts the species concentration at the electrode of the fuel cell under the constraint of uniform current density along the channel. For convenience of use as a formula, the asymptotic solutions to some results are found for two different limits of x/k.

Keywords: Fuel cell; Channel flow; Asymptotic solution; Laplace transform; Draft angle

1. Introduction

Channel flow belongs to the class of most fundamental problems for which the Navier–Stokes equation can be solved exactly. Since every device using fluids needs a fluid supply passage, channel flow has functioned as a simplistic model of the phenomena that occur in complex devices such as catalytic converter–fuel cell assemblies and MEMS devices. Considering its wide applicability and versatility, it might not be possible to enumerate all the applications of channel flow. As models have been developed to incorporate various aspects of physics, techniques to solve them with greater sophistication and speed have also been suggested. However, in spite of the long history of development, most of these models do not allow an analytical approach because of the non-linearity of the governing equation and the coupling between variables.

A fuel cell is an electrochemical energy-conversion device that uses different types of fuel, such as hydrocarbons, methanol and hydrogen. There are various types of fuel cell, depending on the electrolyte, but most of them have a supply channel of reactants to a porous electrode in common. From the perspective of the fuel cell channel, the electrochemical reaction at the electrode can be modeled as suction of reactants and injection of product species through the bottom of the channel. The channel flow with wall suction or injection without the inclusion of a chemical reaction is well known as the Berman problem. Many researchers have tried to find various types of solutions and the instability modes for the so-called symmetric and asymmetric Berman problems. A two-dimensional velocity profile has been found for the Berman problem with the aid of a similarity function that can be expressed as a series expansion in terms of the Reynolds number based on the injection or suction velocity. Recently, Cox and King [1] reviewed this approach in their findings of more complete asymptotic solutions for the Berman problem. In the field of fuel cells, where electrochemical reactions complicate the channel flow, Kulikovsky [2] analytically found the velocity and species concentration along the channel direction. Using a one-dimensional model and neglecting viscous dissipation, he used a low-Mach-number approximation to remove the non-linearity of the convection term.

In this paper, we propose a two-dimensional reacting flow model for a fuel cell that includes variation of species concentration in the direction of the channel height. The channel is allowed to have a trapezoidal cross-section instead of a rectangular shape so that the model can predict the effect of the draft angle that is common in composite or metal separator plates. In this paper it is assumed that the velocity is not changed by the electrochemical reaction, which can be justified when the concentration of inert gas is exceedingly large compared to that of the species participating in the reaction [2]. This hypothesis

* Tel.: +82 16 729 6849; fax: +82 31 368 6787.
E-mail address: heyman@hyundai-motor.com.

0378-7753/$ – see front matter © 2005 Elsevier B.V. All rights reserved.
doi:10.1016/j.jpowsour.2005.12.009

Nomenclature

A, A'	constant representing the concentration gradient
c	species concentration
C	Laplace transform of c
F	Faraday's constant
h	channel half-height
i	current density
j	index used in the Stehfest algorithm of Eq. (31)
k	parameter defined in Section 3.1
L	Laplace transform
M	number of terms in the Stehfest algorithm of Eq. (31)
$\bar{m}_{\text{wall}}$	mass flux at the bottom wall
O	order of magnitude
p	pressure
Re	Reynolds number
s	Laplace-transformed coordinate of x
Sc	Schmidt number
u	stream-wise velocity
v	transverse velocity
W	channel width
W_0	channel width at $y=0$
$W_{M,n}$	constant defined in Section 4.1
x	non-dimensionalized stream-wise coordinate
y	non-dimensionalized transverse coordinate

Greek letters

β	draft angle parameter defined in Section 2
ε	perturbation parameter
λ	constant defined in Section 2
θ	draft angle

Subscripts

0,(0)	zero order
1,(1)	first order
2,(2)	second order
n	index used in the Stehfest algorithm of Eq. (31)
w	wall condition

Superscripts

i	species i
n	index used in the Stehfest algorithm of Eq. (31)

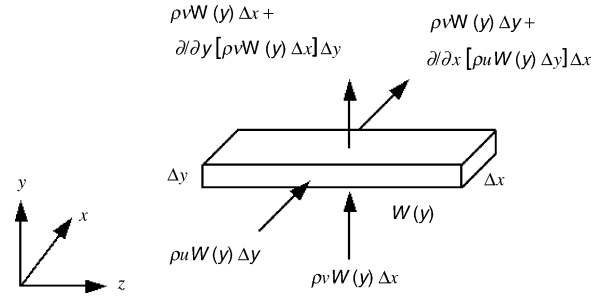

Fig. 2. Infinitesimal control volume for the channel with draft angle θ.

needs to be checked for many examples of real operating conditions, but is adopted for simplicity of the solution in this paper.

2. Mathematical formulation

As a method to investigate the reacting flow in a fuel cell, we use channel flow with a suction or injection boundary condition for a certain species. Fig. 1 shows a schematic diagram of the model that is investigated in this paper. The flow is driven by a pressure gradient formed in the x direction, while a concentration gradient in the y direction imparts additional movement to the species within the channel. In the z direction, there are variations in the velocity and concentration originating from the no-slip and zero-flux boundary condition at the wall. However, its effect is secondary compared with variation in the x and y directions. The fuel cell channel has a small cross-section compared with its length, which often amounts to a few 100 times its cross-section dimension. The channel width $W(y)$ varies with y and can be written as function of the draft angle θ, for which $\theta=0$ corresponds to the rectangular channel case.

In the fuel cell, the suction velocity of the reactant species is a function of the current density divided by the product of the Faraday constant and the concentration of that species [3]. Considering that the average current density of a fuel cell under normal operating conditions is approximately 1 A cm^{-2}, the suction velocity is found to be a tiny fraction of the mainstream velocity U, which is approximately 5 m s^{-1} under the same conditions.

$$|v_w|\ O\left(\frac{i}{Fc^i}\right)\cdots\left|\frac{v_w}{U}\right|\ O(10^{-3}), \qquad \frac{\partial}{\partial y}\gg\frac{\partial}{\partial x}. \tag{1}$$

This observation allows us to assume that diffusion in the y direction will dominate that in the other directions, which is consistent with the boundary layer approximation [4]. Fig. 2 shows the control volume for the trapezoidal channel in Fig. 1,

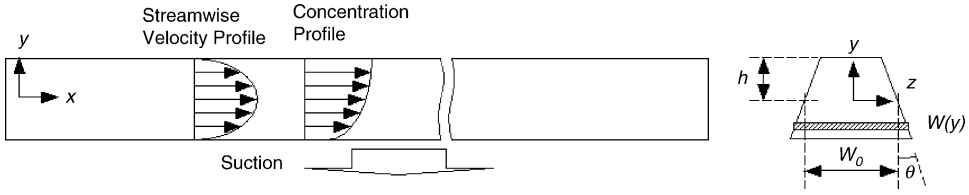

Fig. 1. Schematic diagram of the channel shape and coordinate system under investigation.

together with mass fluxes into and out of each surface. It has finite width $W(y)$, and infinitesimal thickness Δx and height Δy. Taking the limit as $\Delta x \to 0$, $\Delta y \to 0$, the mass balance within the control volume yields:

$$\frac{\partial(Wu)}{\partial x} + \frac{\partial(Wv)}{\partial y} = 0 \tag{2}$$

The momentum and the species balance can be treated in the same manner. As a first approximation to the Maxwell–Stefan equation, the diffusion is considered to follow Fick's law for binary fluids, irrespective of the number of components. The length, velocity, and pressure are non-dimensionalized by the channel half-height h, mean velocity U, and dynamic pressure ρU^2. Neglecting axial diffusion and introducing non-dimensionalized variables, the governing equation for the trapezoidal channel flow with reaction yields:

$$\begin{aligned}
&\bar{W}\frac{\partial u}{\partial x} + \bar{W}\frac{\partial v}{\partial y} + v\frac{\partial \bar{W}}{\partial y} = 0 \\
&\bar{W}u\frac{\partial u}{\partial x} + \bar{W}v\frac{\partial u}{\partial y} = -\bar{W}\frac{\partial p}{\partial x} + \frac{1}{Re}\frac{\partial}{\partial y}\left[\bar{W}\frac{\partial u}{\partial y}\right] \\
&\bar{W}u\frac{\partial c^i}{\partial x} + \bar{W}v\frac{\partial c^i}{\partial y} = \frac{1}{ReSc}\frac{\partial}{\partial y}\left[\bar{W}\frac{\partial c^i}{\partial y}\right]
\end{aligned} \tag{3}$$

The normalized channel width $\bar{W}(y)$ and the draft angle parameter β are defined as follows:

$$\bar{W}(y) = 1 - \beta y \quad (-1 \le y \le 1), \qquad \beta \equiv \frac{2\tan\theta}{W_0/h}$$

where θ is the draft angle, and $W_0 = W(0)$ (4)

Since we assume that the velocity is not changed by the reaction, the momentum equation for the fully developed flow can be simplified as follows:

$$\frac{\partial u}{\partial x} = 0, \qquad v = 0 \cdots Re\frac{\partial p}{\partial x} = \frac{1}{\bar{W}}\frac{\partial}{\partial y}\left[\bar{W}\frac{\partial u}{\partial y}\right] = \text{const} \equiv \lambda \tag{5}$$

From the no-slip boundary condition:

$$u(-1) = u(1) = 0 \tag{6}$$

Expanding u in terms of the draft angle parameter β as a perturbation variable:

$$u = u_{(0)} + \beta u_{(1)} + \beta^2 u_{(2)} + \cdots, \tag{7}$$

where the zero order in β is:

$$\begin{aligned}
&\frac{d^2u_{(0)}}{dy^2} = \lambda, \qquad u_{(0)}(-1) = u_{(0)}(1) = 0 \\
&\therefore u_{(0)} = \frac{\lambda}{2}(y^2 - 1)
\end{aligned} \tag{8}$$

the first order in β is:

$$\begin{aligned}
&\frac{d^2u_{(1)}}{dy^2} = \frac{d}{dy}\left(y\frac{du_{(0)}}{dy}\right) - \lambda y = \lambda y, \\
&u_{(1)}(-1) = u_{(1)}(1) = 0 \qquad \therefore u_{(1)} = \frac{\lambda}{6}(y^3 - y)
\end{aligned} \tag{9}$$

the second order in β is:

$$\begin{aligned}
&\frac{d^2u_{(2)}}{dy^2} = \frac{d}{dy}\left(y\frac{du_{(1)}}{dy}\right) = \frac{\lambda}{3}(2y^3 - y), \\
&u_{(2)}(-1) = u_{(2)}(1) = 0 \qquad \therefore u_{(2)} = \frac{\lambda}{90}(3y^5 - 5y^3 + 2y)
\end{aligned} \tag{10}$$

and the third order in β is:

$$\begin{aligned}
&\frac{d^2u_{(3)}}{dy^2} = \frac{d}{dy}\left(y\frac{du_{(2)}}{dy}\right) = \frac{\lambda}{90}(75y^4 - 45y^2 + 2), \\
&u_{(3)}(-1) = u_{(3)}(1) = 0 \\
&\therefore u_{(3)} = \frac{\lambda}{360}(10y^6 - 15y^4 + 4y^2 + 1)
\end{aligned} \tag{11}$$

Collecting and adding terms up to the third order gives:

$$\begin{aligned}
u \approx\ & \frac{\lambda}{2}(y^2 - 1) + \beta\frac{\lambda}{6}(y^3 - y) + \beta^2\frac{\lambda}{90}(3y^5 - 5y^3 + 2y) \\
&+\beta^3\frac{\lambda}{360}(10y^6 - 15y^4 + 4y^2 + 1)
\end{aligned} \tag{12}$$

The constant λ is calculated from the definition of the average velocity:

$$1 = \frac{1}{2}\int_{-1}^{1} u\,dy \approx \frac{1}{2}\int_{-1}^{1} u_{(0)}\,dy = -\frac{\lambda}{3} \qquad \therefore \lambda \approx -3 \tag{13}$$

Fig. 3 shows the change in velocity profile with draft angle varied up to 40° for the case $W_0/h = 2$. The location of the peak velocity moves upward as the draft angle increases because of the reduction in the effective area in the upper region of channel.

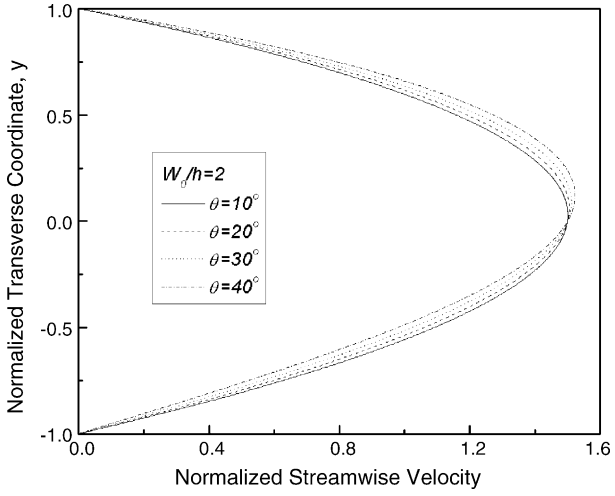

Fig. 3. Effect of draft angle θ on normalized velocity profile within the channel.

This is the result for $W_0/h = 2$, in other words for a channel with square cross-section when it has no draft angle. If the channel has greater width than its height, the effect of the draft angle will be lessened, as can be deduced from the definition of β.

Using Eqs. (12) and (13), the species equation now can be simplified as follows:

$$\bar{W}u\frac{\partial c^i}{\partial x} = \frac{1}{ReSc}\frac{\partial}{\partial y}\left[\bar{W}\frac{\partial c^i}{\partial y}\right]$$

$$\text{where } u \approx u_{(0)} + \beta u_{(1)} + \beta^2 u_{(2)} + \beta^3 u_{(3)} + \cdots \tag{14}$$

As for the boundary condition, the inlet concentration is assumed to be constant. To simplify the calculation, we redefine the concentration c^i as deviation from the inlet condition. In spite of this change, Eq. (14) can still be used in its original form, since it contains only derivative terms. At the reacting wall of the bottom, the Neumann-type boundary condition can be imposed under the assumption that mass transfer there occurs only by diffusion. If the channel has a meandering shape or a dead-end configuration, the pressure rise in the channel will be high enough to allow the direct penetration of species into the electrode. In that case, we have to include convective transport into the wall, which requires simultaneous solution of the y-momentum equation. To simplify the solution, we assume a straight channel that has negligible pressure drop along the channel. Since the total flux of suction or injection is determined by external loading and is not dependent on the change in the bottom area of channel caused by draft, the following condition is imposed on the bottom surface:

$$\bar{m}_{\text{wall}} \sim \bar{W}_{y=-1}\left(\frac{\partial c^i}{\partial y}\right)_{y=-1} \qquad \therefore \left(\frac{\partial c^i}{\partial y}\right)_{y=-1}$$

$$= \frac{A}{1+\beta} \quad \text{where } A \sim \bar{m}_{\text{wall}} \tag{15}$$

At the upper, non-reacting wall, there will be no mass flux of any kind, which means that the concentration gradient vanishes there. To sum up:

$$c^i\big|_{x=0} = 0, \qquad \left.\frac{\partial c^i}{\partial y}\right|_{y=-1} = \frac{A}{1+\beta}, \qquad \left.\frac{\partial c^i}{\partial y}\right|_{y=1} = 0 \tag{16}$$

If A is positive, suction of species i occurs at the wall, whereas if it is negative, injection occurs. The magnitude of A is related to the amount of suction or injection of species i and consequently to the local current density by Faraday's law. Under most operating conditions for fuel cells, except at very low current density, A varies along x and should be simultaneously determined with the other variables. Although the current density is sometimes assumed to have a certain profile, such as an exponentially decreasing function [2], or to have constant value [5], it is obvious that assumption of the condition of constant A is not well supported by experiments in most cases. However, we adopt it in this paper to concentrate on the flow and mass transfer while considering the electrochemical reaction only through the suction or injection boundary condition.

The concentration of species i, more exactly the concentration change for species i from the inlet condition, can be expanded in terms of β as in the case of velocity:

$$c^i = c^i_{(0)} + \beta c^i_{(1)} + \beta^2 c^i_{(2)} + \beta^3 c^i_{(3)} + \cdots \tag{17}$$

Expanding Eqs. (14) and (16) similarly and collecting like terms of β, the following equations and boundary conditions are obtained after substitution into Eqs. (8)–(11).

Zero-order terms in β:

$$k(1-y^2)\frac{\partial c^i_{(0)}}{\partial x} = \frac{\partial^2 c^i_{(0)}}{\partial y^2} \quad \text{where } k \equiv \frac{3}{2}ReSc \tag{18}$$

$$c^i_{(0)}\big|_{x=0} = 0, \qquad \left.\frac{\partial c^i_{(0)}}{\partial y}\right|_{y=-1} = \frac{A}{1+\beta}, \qquad \left.\frac{\partial c^i_{(0)}}{\partial y}\right|_{y=1} = 0 \tag{19}$$

First-order terms in β:

$$k(1-y^2)\frac{\partial c^i_{(1)}}{\partial x} - \frac{\partial^2 c^i_{(1)}}{\partial y^2} = -\frac{\partial c^i_{(0)}}{\partial y} - \frac{1}{3}y\frac{\partial^2 c^i_{(0)}}{\partial y^2} \tag{20}$$

$$c^i_{(1)}\big|_{x=0} = 0, \qquad \left.\frac{\partial c^i_{(1)}}{\partial y}\right|_{y=-1} = 0, \qquad \left.\frac{\partial c^i_{(1)}}{\partial y}\right|_{y=1} = 0 \tag{21}$$

Second-order terms in β:

$$k(1-y^2)\frac{\partial c^i_{(2)}}{\partial x} - \frac{\partial^2 c^i_{(2)}}{\partial y^2} = -\frac{\partial c^i_{(1)}}{\partial y} - \frac{y}{3}\frac{\partial^2 c^i_{(1)}}{\partial y^2} - \frac{2y}{3}\frac{\partial c^i_{(0)}}{\partial y}$$
$$+\frac{2y}{90}(2+5y-3y^2)\frac{\partial^2 c^i_{(0)}}{\partial y^2} \tag{22}$$

$$c^i_{(2)}\big|_{x=0} = 0, \qquad \left.\frac{\partial c^i_{(2)}}{\partial y}\right|_{y=-1} = 0, \qquad \left.\frac{\partial c^i_{(2)}}{\partial y}\right|_{y=1} = 0 \tag{23}$$

Third-order terms in β:

$$k(1-y^2)\frac{\partial c^i_{(3)}}{\partial x} - \frac{\partial^2 c^i_{(3)}}{\partial y^2}$$
$$= -\frac{\partial c^i_{(2)}}{\partial y} - \frac{y}{3}\frac{\partial^2 c^i_{(2)}}{\partial y^2} - \frac{2y}{3}\frac{\partial c^i_{(1)}}{\partial y} + \frac{y}{45}(2+5y-3y^2)\frac{\partial^2 c^i_{(1)}}{\partial y^2}$$
$$-\frac{y}{45}(2+35y-3y^2)\frac{\partial c^i_{(0)}}{\partial y}$$
$$+\frac{1}{540}(3-y^2-20y^3-6y^4)\frac{\partial^2 c^i_{(0)}}{\partial y^2} \tag{24}$$

$$c^i_{(3)}\big|_{x=0} = 0, \qquad \left.\frac{\partial c^i_{(3)}}{\partial y}\right|_{y=-1} = 0, \qquad \left.\frac{\partial c^i_{(3)}}{\partial y}\right|_{y=1} = 0 \tag{25}$$

3. Numerical results

3.1. The perturbation method

In this section, we use the perturbation method and the Laplace transform technique to systematically investigate Eqs.

(18)–(25). The perturbation method in this section is different from that used in Section 2, in that the perturbation parameter ε has no physical meaning, but is introduced for mathematical convenience. Eqs. (18), (20), (22) and (24) commonly contain the term y^2 on the left-hand side, the omission of which greatly simplifies the solution. Hence, we multiply the term y^2 by the perturbation parameter ε and expand the left-hand side in terms of ε, while the right-hand side is calculated from the solutions for the lower-order equations. After solving the decomposed equations, they are recombined with the substitution of 1 for the perturbation parameter ε. This approach can be regarded as being valid as far as the recombined terms constitute a converged series [6,7].

3.1.1. Zero-order terms in β

$$k(1-\varepsilon y^2)\frac{\partial c^i_{(0)}}{\partial x} = \frac{\partial^2 c^i_{(0)}}{\partial y^2}$$

$$\text{where } c^i_{(0)} = c_0 + \varepsilon c_1 + \varepsilon^2 c_2 + \cdots \tag{26}$$

Zero-order terms in ε:

$$k\frac{\partial c_0}{\partial x} = \frac{\partial^2 c_0}{\partial y^2}, \qquad c_0|_{x=0} = 0, \qquad \left.\frac{\partial c_0}{\partial y}\right|_{y=-1} = \frac{A}{1+\beta},$$

$$\left.\frac{\partial c_0}{\partial y}\right|_{y=1} = 0 \tag{27}$$

For terms of order j larger than 0:

$$k\frac{\partial c_j}{\partial x} - \frac{\partial^2 c_j}{\partial y^2} = ky^2\frac{\partial c_{j-1}}{\partial x}, \qquad c_j|_{x=0} = 0, \qquad \left.\frac{\partial c_j}{\partial y}\right|_{y=-1} = 0,$$

$$\left.\frac{\partial c_j}{\partial y}\right|_{y=1} = 0 \quad \text{where } j = 1, 2, 3, \cdots \tag{28}$$

3.1.2. First-order terms in β

$$k(1-\varepsilon y^2)\frac{\partial c^i_{(1)}}{\partial x} - \frac{\partial^2 c^i_{(1)}}{\partial y^2} = -\frac{\partial c^i_{(0)}}{\partial y} - \frac{y}{3}\frac{\partial^2 c^i_{(0)}}{\partial y^2}$$

$$\text{where } c^i_{(1)} = c_0 + \varepsilon c_1 + \varepsilon^2 c_2 + \cdots \tag{29}$$

Zero-order terms in ε:

$$k\frac{\partial c_0}{\partial x} - \frac{\partial^2 c_0}{\partial y^2} = -\frac{\partial c^i_{(0)}}{\partial y} - \frac{y}{3}\frac{\partial^2 c^i_{(0)}}{\partial y^2}, \qquad c_0|_{x=0} = 0,$$

$$\left.\frac{\partial c_0}{\partial y}\right|_{y=-1} = 0, \qquad \left.\frac{\partial c_0}{\partial y}\right|_{y=1} = 0 \tag{30}$$

For terms of order j larger than 0:

$$k\frac{\partial c_j}{\partial x} - \frac{\partial^2 c_j}{\partial y^2} = ky^2\frac{\partial c_{j-1}}{\partial x}, \qquad c_j|_{x=0} = 0,$$

$$\left.\frac{\partial c_j}{\partial y}\right|_{y=-1} = 0, \qquad \left.\frac{\partial c_j}{\partial y}\right|_{y=1} = 0 \quad \text{where } j = 1, 2, 3, \cdots \tag{31}$$

3.1.3. Second-order terms in β

$$k(1-\varepsilon y^2)\frac{\partial c^i_{(2)}}{\partial x} - \frac{\partial^2 c^i_{(2)}}{\partial y^2} = -\frac{\partial c^i_{(1)}}{\partial y} - \frac{y}{3}\frac{\partial^2 c^i_{(1)}}{\partial y^2} - \frac{2y}{3}\frac{\partial c^i_{(0)}}{\partial y} + \frac{2y}{90}(2+5y-3y^2)\frac{\partial^2 c^i_{(0)}}{\partial y^2}$$

$$\text{where } c^i_{(2)} = c_0 + \varepsilon c_1 + \varepsilon^2 c_2 + \cdots \tag{32}$$

Zero-order terms in ε:

$$k\frac{\partial c_0}{\partial x} - \frac{\partial^2 c_0}{\partial y^2} = -\frac{\partial c^i_{(1)}}{\partial y} - \frac{y}{3}\frac{\partial^2 c^i_{(1)}}{\partial y^2} - \frac{2y}{3}\frac{\partial c^i_{(0)}}{\partial y} + \frac{2y}{90}(2+5y-3y^2)\frac{\partial^2 c^i_{(0)}}{\partial y^2}, \qquad c_0|_{x=0} = 0,$$

$$\left.\frac{\partial c_0}{\partial y}\right|_{y=-1} = 0, \qquad \left.\frac{\partial c_0}{\partial y}\right|_{y=1} = 0 \tag{33}$$

For terms of order j larger than 0:

$$k\frac{\partial c_j}{\partial x} - \frac{\partial^2 c_j}{\partial y^2} = ky^2\frac{\partial c_{j-1}}{\partial x}, \qquad c_j|_{x=0} = 0,$$

$$\left.\frac{\partial c_j}{\partial y}\right|_{y=-1} = 0, \qquad \left.\frac{\partial c_j}{\partial y}\right|_{y=1} = 0 \quad \text{where } j = 1, 2, 3, \cdots \tag{34}$$

3.1.4. Third-order terms in β

$$k(1-\varepsilon y^2)\frac{\partial c^i_{(3)}}{\partial x} - \frac{\partial^2 c^i_{(3)}}{\partial y^2} = -\frac{\partial c^i_{(2)}}{\partial y} - \frac{y}{3}\frac{\partial^2 c^i_{(2)}}{\partial y^2} - \frac{2y}{3}\frac{\partial c^i_{(1)}}{\partial y} + \frac{y(2+5y-3y^2)}{45}\frac{\partial^2 c^i_{(1)}}{\partial y^2} - \frac{y(2+35y-3y^2)}{45}\frac{\partial c^i_{(0)}}{\partial y} + \frac{3-y^2-20y^3-6y^4}{540}\frac{\partial^2 c^i_{(0)}}{\partial y^2}$$

$$\text{where } c^i_{(3)} = c_0 + \varepsilon c_1 + \varepsilon^2 c_2 + \cdots \tag{35}$$

Zero-order terms in ε:

$$k\frac{\partial c_0}{\partial x} - \frac{\partial^2 c_0}{\partial y^2} = -\frac{\partial c^i_{(2)}}{\partial y} - \frac{y}{3}\frac{\partial^2 c^i_{(2)}}{\partial y^2} - \frac{2y}{3}\frac{\partial c^i_{(1)}}{\partial y} + \frac{y(2+5y-3y^2)}{45}\frac{\partial^2 c^i_{(1)}}{\partial y^2} - \frac{y(2+35y-3y^2)}{45}\frac{\partial c^i_{(0)}}{\partial y} + \frac{3-y^2-20y^3-6y^4}{540}\frac{\partial^2 c^i_{(0)}}{\partial y^2}, \qquad c_0|_{x=0} = 0,$$

$$\left.\frac{\partial c_0}{\partial y}\right|_{y=-1} = 0, \qquad \left.\frac{\partial c_0}{\partial y}\right|_{y=1} = 0 \tag{36}$$

For terms of order j larger than 0:

$$k\frac{\partial c_j}{\partial x} - \frac{\partial^2 c_j}{\partial y^2} = ky^2\frac{\partial c_{j-1}}{\partial x}, \qquad c_j\big|_{x=0} = 0,$$
$$\left.\frac{\partial c_j}{\partial y}\right|_{y=-1} = 0, \quad \left.\frac{\partial c_j}{\partial y}\right|_{y=1} = 0 \quad \text{where } j = 1, 2, 3, \cdots \tag{37}$$

3.2. The Laplace transform

The partial differential equations that were derived in the previous section can be transformed to ordinary differential equations (ODEs) using the Laplace transform, the definition of which can be expressed as follows:

$$C_j(s, y) \equiv L[c_j(x, y)] = \int_0^\infty \mathrm{e}^{-sx} c_j(x, y)\,\mathrm{d}x,$$
$$\text{where } j = 0, 1, 2, \cdots \tag{38}$$

3.2.1. Zero-order terms in β

$$C_{(0)} \equiv L[c^i_{(0)}] = C_0 + \varepsilon C_1 + \varepsilon^2 C_2 + \cdots \tag{39}$$

Zero-order terms in ε:

$$ksC_0(s, y) = \frac{\mathrm{d}^2 C_0(s, y)}{\mathrm{d}y^2},$$
$$\left.\frac{\mathrm{d}C_0}{\mathrm{d}y}\right|_{y=-1} = \frac{A}{1+\beta}\frac{1}{s}, \qquad \left.\frac{\mathrm{d}C_0}{\mathrm{d}y}\right|_{y=1} = 0 \tag{40}$$

For terms of order j larger than 0:

$$ksC_j(s, y) - \frac{\mathrm{d}^2 C_j(s, y)}{\mathrm{d}y^2} = ksy^2 C_{j-1}(s, y),$$
$$\left.\frac{\mathrm{d}C_j}{\mathrm{d}y}\right|_{y=-1} = 0, \qquad \left.\frac{\mathrm{d}C_j}{\mathrm{d}y}\right|_{y=1} = 0 \tag{41}$$

3.2.2. First-order terms in β

$$C_{(1)} \equiv L[c^i_{(1)}] = C_0 + \varepsilon C_1 + \varepsilon^2 C_2 + \cdots \tag{42}$$

Zero-order terms in ε:

$$ksC_0 - \frac{\mathrm{d}^2 C_0}{\mathrm{d}y^2} = -\frac{\mathrm{d}C_{(0)}}{\mathrm{d}y} - \frac{y}{3}\frac{\mathrm{d}^2 C_{(0)}}{\mathrm{d}y^2},$$
$$\left.\frac{\mathrm{d}C_0}{\mathrm{d}y}\right|_{y=-1} = 0, \qquad \left.\frac{\mathrm{d}C_0}{\mathrm{d}y}\right|_{y=1} = 0 \tag{43}$$

For terms of order j larger than 0:

$$ksC_j(s, y) - \frac{\mathrm{d}^2 C_j(s, y)}{\mathrm{d}y^2} = ksy^2 C_{j-1}(s, y),$$
$$\left.\frac{\mathrm{d}C_j}{\mathrm{d}y}\right|_{y=-1} = 0, \qquad \left.\frac{\mathrm{d}C_j}{\mathrm{d}y}\right|_{y=1} = 0. \tag{44}$$

3.2.3. Second-order terms in β

$$C_{(2)} \equiv L[c^i_{(2)}] = C_0 + \varepsilon C_1 + \varepsilon^2 C_2 + \cdots \tag{45}$$

Zero-order terms in ε:

$$ksC_0 - \frac{\mathrm{d}^2 C_0}{\mathrm{d}y^2} = -\frac{\mathrm{d}C_{(1)}}{\mathrm{d}y} - \frac{y}{3}\frac{\mathrm{d}^2 C_{(1)}}{\mathrm{d}y^2} - \frac{2y}{3}\frac{\mathrm{d}C_{(0)}}{\mathrm{d}y} + \frac{2y}{90}(2 + 5y - 3y^2)\frac{\mathrm{d}^2 C_{(0)}}{\mathrm{d}y^2},$$
$$\left.\frac{\mathrm{d}C_0}{\mathrm{d}y}\right|_{y=-1} = 0, \qquad \left.\frac{\mathrm{d}C_0}{\mathrm{d}y}\right|_{y=1} = 0 \tag{46}$$

For terms of order j larger than 0:

$$ksC_j(s, y) - \frac{\mathrm{d}^2 C_j(s, y)}{\mathrm{d}y^2} = ksy^2 C_{j-1}(s, y),$$
$$\left.\frac{\mathrm{d}C_j}{\mathrm{d}y}\right|_{y=-1} = 0, \qquad \left.\frac{\mathrm{d}C_j}{\mathrm{d}y}\right|_{y=1} = 0 \tag{47}$$

3.2.4. Third-order terms in β

$$C_{(3)} \equiv L[c^i_{(3)}] = C_0 + \varepsilon C_1 + \varepsilon^2 C_2 + \cdots \tag{48}$$

Zero-order terms in ε:

$$ksC_0 - \frac{\mathrm{d}^2 C_0}{\mathrm{d}y^2} = -\frac{\mathrm{d}C_{(2)}}{\mathrm{d}y} - \frac{y}{3}\frac{\mathrm{d}^2 C_{(2)}}{\mathrm{d}y^2} - \frac{2y}{3}\frac{\mathrm{d}C_{(1)}}{\mathrm{d}y} + \frac{y(2 + 5y - 3y^2)}{45}\frac{\mathrm{d}^2 C_{(1)}}{\mathrm{d}y^2} - \frac{y(2 + 35y - 3y^2)}{45}\frac{\mathrm{d}C_{(0)}}{\mathrm{d}y} + \frac{3 - y^2 - 20y^3 - 6y^4}{540}\frac{\mathrm{d}^2 C_{(0)}}{\mathrm{d}y^2},$$
$$\left.\frac{\mathrm{d}C_0}{\mathrm{d}y}\right|_{y=-1} = 0, \ \left.\frac{\mathrm{d}C_0}{\mathrm{d}y}\right|_{y=1} = 0 \tag{49}$$

For terms of order j larger than 0:

$$ksC_j(s, y) - \frac{\mathrm{d}^2 C_j(s, y)}{\mathrm{d}y^2} = ksy^2 C_{j-1}(s, y),$$
$$\left.\frac{\mathrm{d}C_j}{\mathrm{d}y}\right|_{y=-1} = 0, \qquad \left.\frac{\mathrm{d}C_j}{\mathrm{d}y}\right|_{y=1} = 0 \tag{50}$$

3.3. Solution of ODEs and the inverse Laplace transform

The ODEs derived in the previous section can be solved analytically by successive substitution. However, the inverse Laplace transforms for these are nearly impossible to find directly using the conversion formula. The Stehfest algorithm [8,9] is an effective method to find the inverse Laplace trans-

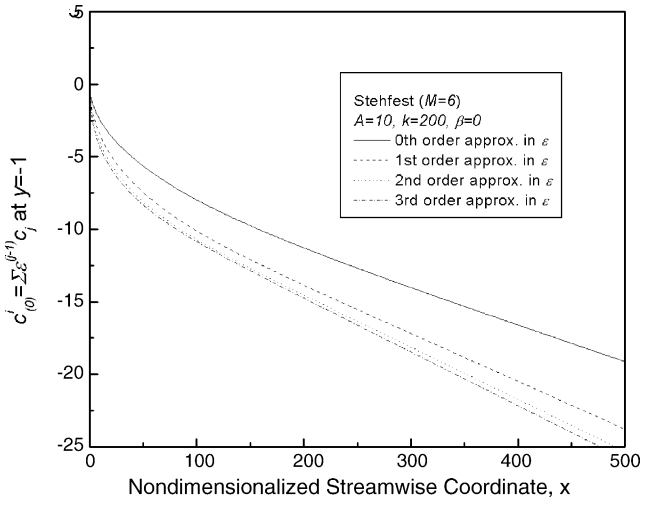

Fig. 4. Change in $C^i_{(0)}(x, 1)$ as the order of approximation in ε is changed ($A = 10$, $k = 200$, $\beta = 0$). Exact solutions to ODEs for C_j were used in the inverse Laplace transform with $M = 6$ for the Stehfest algorithm.

forms approximately:

$$c_i(x, y) \approx \frac{\ln 2}{x}\sum_{j=1}^{M} w_j C_i(s_j, y) \quad \text{where } s_j = j\frac{\ln 2}{x}$$

$$w_j = (-1)^{M/2+j}\sum_{n=(1+j)/2}^{\min(j,M/2)} \frac{(2n)!n^{M/2}}{(M/2-n)!n!(n-1)!(j-n)!(2n-j)!} \tag{51}$$

The number of terms M in the Stehfest algorithm is usually set higher than or equal to six [10]. In this section, we provide some results using the internal functions of Mathematica to treat the ODEs and the additional package developed by Cheng et al. [11] in implementing the Stehfest algorithm. The number of terms to be included in the expansion for the desired accuracy is also checked before we try to find the analytical solution.

Let us consider a polymer electrolyte membrane (PEM) fuel cell under normal operating conditions of 1 atm and 80 °C. The fuel cell is assumed to operate under uniform current density mode at approximately 1 A cm^{-2}. The stoichiometric ratio, which represents how many times reactants are supplied through the inlet compared to the quantity that actually participates in the reaction, is ordinarily set higher than or equal to 2.0. The channel cross-section within the separator plate is considered to have a square shape with height and width equal to 2 mm, and its length to be much greater, as for most serpentine channel shapes. Let us assume that the ratio of the channel length to its height is 250, in other words the channel length non-dimensionalized by the channel half-height h is 500. For this channel shape and these operating conditions, the Reynolds number is approximately 200. The Schmidt number for different gas pairs is 0.56–0.74 for N_2, O_2, and H_2O compounds [12]. Hence, k in Eq. (18) is approximately 200–260, while x varies from 0 to 500. Fig. 4 presents the concentration profile along the channel in the case of no draft as the order of approximation in ε is changed. In the case of no draft, the zero-order term in β, $C^i_{(0)}$ represents c^i. Fig. 4 shows that $C^i_{(0)}$ converges with the inclusion of higher-order terms in ε, and for the first-order approximation it approaches the converged solution with 8% error on average. For the second-order approximation in ε, a 2% error applies to $C^i_{(0)}$ on average. From this result, we choose to cut off the terms higher than the second order in ε in this paper. Fig. 5 presents the concentration profile for the channel with non-zero draft angle with the order of approximation in β changed. The result presented is for conditions of $A = 10$, $k = 200$, and $\theta = 10°$. It shows that the first-order approximation in β is sufficient to provide an accurate profile of c^i in the case of non-zero draft. Fig. 6 shows the error of the first-order approximation compared to the third-order approximation at various locations of the channel. Within 3% across the channel length, the first-order approximation in β provides a good representation of higher-order approximations to the converged solution. Fig. 7 plots the concentration change for species i from the inlet condition in the case of no draft. The monitoring point is at the reaction site located at $y = -1$ along the channel width and k is varied from 100 to 500. Excluding the rapid decay near the inlet, the concentration decreases with constant slope along the channel in the case of suction. The slope of the decrease becomes less steep with higher k, the product of the Reynolds number and the Schmidt number. For injection of species i, its concentration would increase along the channel and the slope of the profile would decrease as k increases. It can be deduced from the graph that both increased inertia and enhanced mass diffusion can be used for greater compensation of the concentration change at the reaction site. Fig. 8 shows the change in concentration profile within the channel as k is increased. The graph shows obvious variation in its magnitude

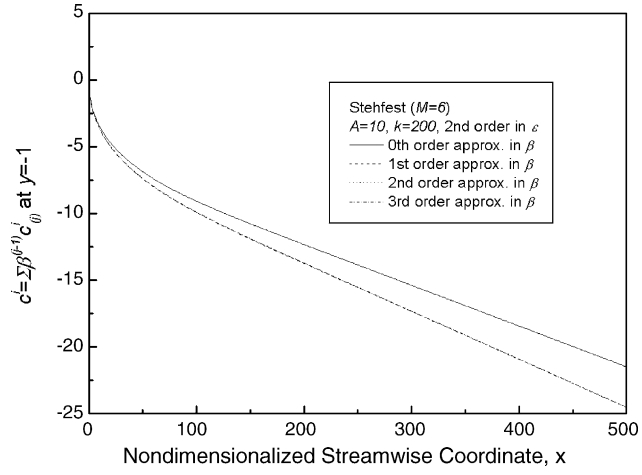

Fig. 5. Change in $c^i(x,-1)$ as the order of approximation in β is changed ($A = 10$, $k = 200$, $\theta = 10°$). Exact solutions to ODEs for C_j were used in the inverse Laplace transform with $M = 6$ for Stehfest algorithm.

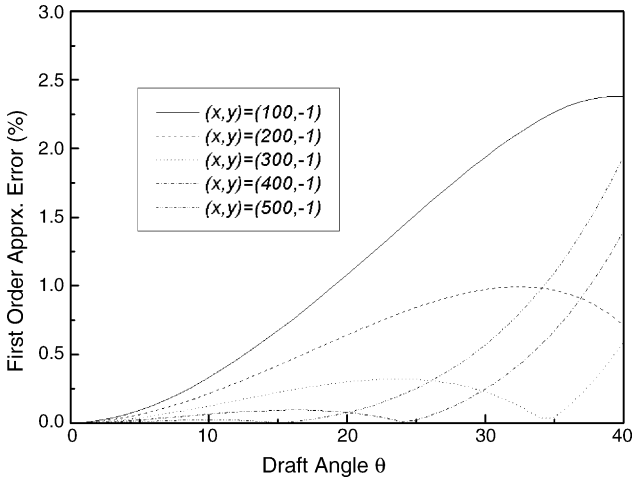

Fig. 6. First-order approximation error in β at various locations of the reaction site.

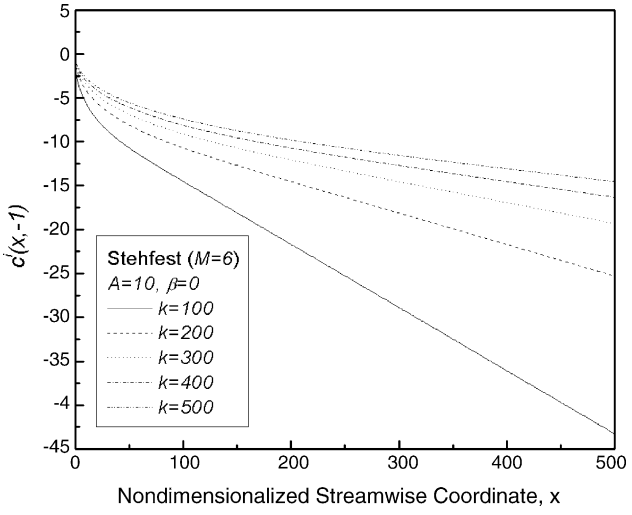

Fig. 7. Concentration change for species i from the inlet condition, $c^i(x,-1)$, as k is increased ($A=10$, $\beta=0$).

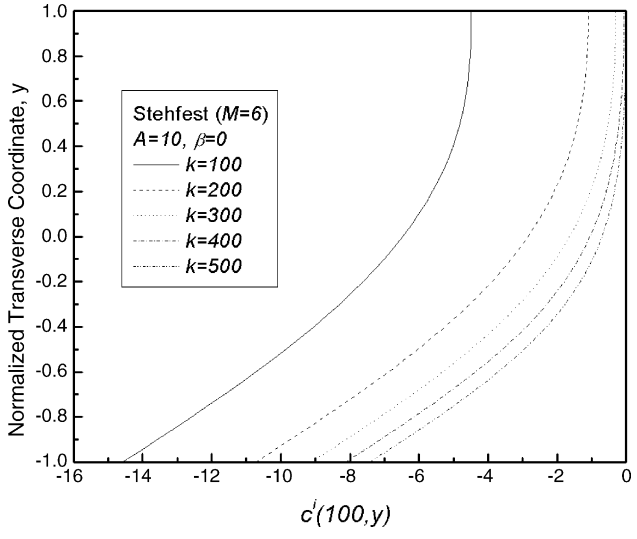

Fig. 8. Concentration change for species i from the inlet condition, $c^i(100,y)$, as k is increased ($A=10$, $\beta=0$).

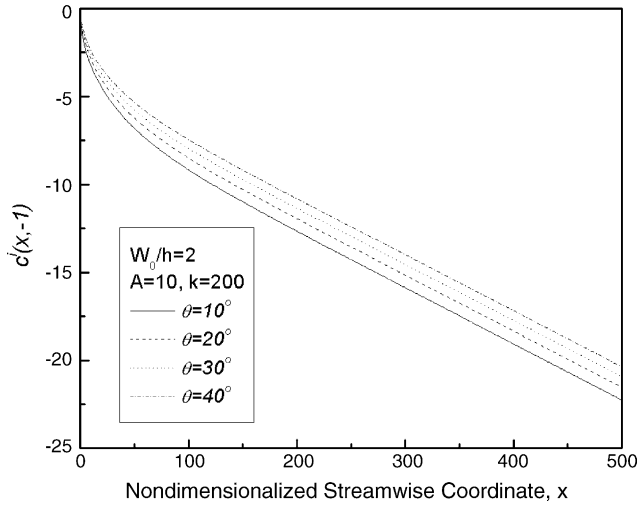

Fig. 9. Effect of draft angle θ on the distribution of concentration $c^i(x,-1)$ in the stream-wise direction ($W_0/h=2$, $A=10$, $k=200$).

in the direction of the channel height, which justifies the use of a two-dimensional model for concentration. For k above 300, the upper wall is hardly affected by reaction at the bottom. This observation suggests that the measurement of species concentration through the slot of the upper wall may not be sufficient to deduce the condition at the bottom. Figs. 9 and 10 show the draft angle effect on the concentration c^i in the directions of the channel length and height. Fig. 11 presents the contour plot for c^i within the channel for two different draft angles. The bigger draft angle produces smaller perturbation of the concentration at the bottom, which means the higher concentration of reactant and the faster removal of product from the reaction site. In the fuel cell, the enhanced activity of reactant oxygen surely contributes to the increase in performance. However, the fast removal of product water may cause membrane drying, which would reduce proton conductivity and lower the performance when operated under low humidity conditions. In the case of high humidity conditions, the removal of product water is favor-

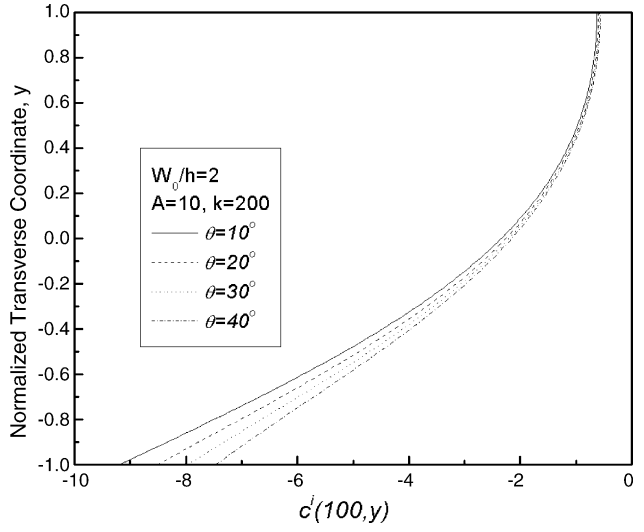

Fig. 10. Effect of draft angle θ on the distribution of concentration deviation $c^i(100,y)$ in the direction of the channel height ($W_0/h=2$, $A=10$, $k=200$).

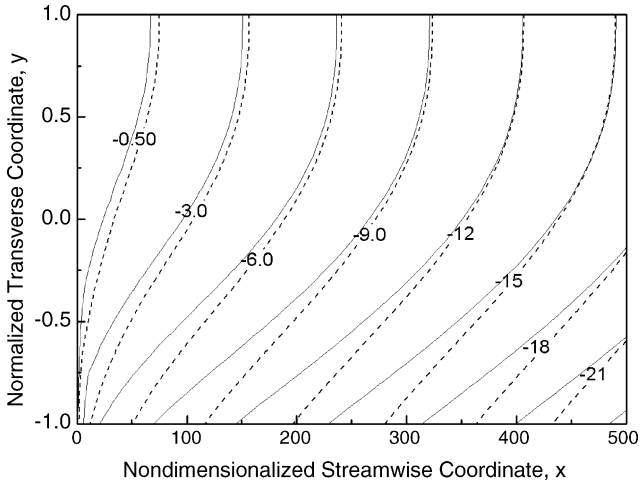

Fig. 11. Concentration change for species i from the inlet condition, $c^i(x,y)$, within the channel for different draft angles: (a) $\theta = 10^\circ$ (solid line); and (b) $\theta = 40^\circ$ (dashed line).

able, but if condensation starts to occur, the reduced momentum at the bottom due to the draft may not be sufficient to withdraw water droplets at the interface with the gas diffusion layer. More details on the water problem for fuel cells can be found in the literature [13–17].

4. Approximate analytical solution

In this section, we try to find the approximate analytical expression for the numerical results presented in Section 3. First, we use two different limits to approximate the ODE solutions and then find their inverse Laplace transforms. From the results presented in Figs. 5 and 6, we determine to expand c^i only up to the first order in β. The analytical solutions for ODEs in this section were found using Mathematica implementing the symbolic operation.

4.1. Asymptotic solutions for ODEs

4.1.1. Small ks limit

For zero-order terms in β, $C_{(0)}$ that satisfies Eqs. (39)–(41) has the following approximate expression at $y = -1$ for small values of ks:

$$C_{(0)} \approx -\frac{Ak}{1+\beta}\left[\frac{13}{18k^2s^2} + \frac{46}{63ks}\right] \tag{52}$$

For first-order terms in β, $C_{(1)}$ that satisfies Eqs. (42)–(44) has the following approximate expression at $y = -1$ for small values of ks:

$$C_{(1)} \approx -\frac{Ak}{1+\beta}\left[\frac{13}{18k^2s^2} + \frac{572}{2835ks}\right] \tag{53}$$

4.1.2. Large ks limit

For zero-order terms in β, $C_{(0)}$ that satisfies Eqs. (39)–(41) has the following approximate expression at $y = -1$ for large values of ks:

$$C_{(0)}(s,-1) \approx -\frac{Ak}{1+\beta}\sum_{n=3}^{7}\frac{\alpha_n}{k^{n/2}s^{n/2}}, \quad \alpha_3 = 1.875,$$
$$\alpha_4 = -1.5, \quad \alpha_5 = 1.75, \quad \alpha_6 = -1.375, \quad \alpha_7 = 0.65625 \tag{54}$$

For first-order terms in β, $C_{(1)}$ that satisfies Eqs. (42)–(44) has the following approximate expression at $y = -1$ for large values of ks:

$$C_{(1)}(s,-1) \approx -\frac{Ak}{1+\beta}\sum_{n=3}^{12}\frac{\alpha_n}{k^{n/2}s^{n/2}}, \quad \alpha_3 = 0.277344,$$
$$\alpha_4 = 1.05859, \quad \alpha_5 = -1.42839, \quad \alpha_6 = 2.44596,$$
$$\alpha_7 = -4.14128, \quad \alpha_8 = 7.82894, \quad \alpha_9 = -13.6265,$$
$$\alpha_{10} = 19.1652, \quad \alpha_{11} = -18.6228, \quad \alpha_{12} = 9.28491 \tag{55}$$

Table 1
$W_{M,n}$ for $M \geq 16$

n	$W_{M,n}$
1	1
3/2	0.939437
2	0.693147
5/2	0.434112
3	0.240227
7/2	0.120362
4	0.0555044
9/2	0.0238368
5	0.00961786
11/2	0.00367086
6	0.00133253

4.2. Approximate inverse Laplace transform

Now we use the Stehfest algorithm of Eq. (51) to find the inverse Laplace transforms for Eqs. (52) and (53), and Eqs. (54) and (55). For convenience, we introduce a new constant, $W_{M,n}$:

$$W_{M,n} \equiv \sum_{j=1}^{M}\frac{w_j}{j^n} \tag{56}$$

For $M \geq 16$, $W_{M,n}$ becomes nearly independent of M, the numerical value of which is tabulated in Table 1 for different values of n.

4.2.1. Small ks limit (large x/k limit)

This limit corresponds to the case of large x/k.

The zero-order terms in β from Eqs. (51) and (52) are:

$$c^i_{(0)}(x,-1) \approx -\frac{A}{1+\beta}\left[\frac{13W_{M,2}}{18\ln 2}\left(\frac{x}{k}\right) + \frac{46W_{M,1}}{63}\right] \tag{57}$$

and the first-order terms in β from Eqs. (51) and (53) are:

$$c^i_{(1)}(x,-1) \approx -\frac{A}{1+\beta}\left[\frac{13W_{M,2}}{18\ln 2}\left(\frac{x}{k}\right) + \frac{572W_{M,1}}{2835}\right] \tag{58}$$

To sum up, for large x/k:

$$c^i(x,-1) \approx c^i_{(0)}(x,-1) \text{ of Eq. (57)} + \beta c^i_{(1)}(x,-1) \text{ of Eq. (58)} \tag{59}$$

$$\therefore c^i(x,-1) \approx -A\left[0.722\left(\frac{x}{k}\right) + 0.730 f(\beta)\right]$$

$$\text{where } f(\beta) = \frac{1+0.2763\beta}{1+\beta} \tag{60}$$

4.2.2. Large ks limit (small x/k limit)

The zero-order terms in β from Eqs. (51) and (54) are:

$$c^i_{(0)}(x,-1) \approx -\frac{A}{1+\beta}\sum_{n=3}^{7}\left[\frac{W_{M,n/2}\alpha_n}{(\ln 2)^{n/2-1}}\left(\frac{x}{k}\right)^{n/2-1}\right],$$

$$\alpha_3 = 1.875, \quad \alpha_4 = -1.5, \quad \alpha_5 = 1.75, \quad \alpha_6 = -1.375,$$

$$\alpha_7 = 0.65625 \tag{61}$$

and the first-order terms in β from Eqs. (51) and (55) are:

$$c^i_{(1)}(x,-1) \approx -\frac{A}{1+\beta}\sum_{n=3}^{12}\frac{W_{M,n/2}\alpha_n}{(\ln 2)^{n/2-1}}\left(\frac{x}{k}\right)^{n/2-1},$$

$$\alpha_3 = 0.277344, \quad \alpha_4 = 1.05859, \quad \alpha_5 = -1.42839,$$

$$\alpha_6 = 2.44596, \quad \alpha_7 = -4.14128, \quad \alpha_8 = 7.82894,$$

$$\alpha_9 = -13.6265, \quad \alpha_{10} = 19.1652, \quad \alpha_{11} = -18.6228,$$

$$\alpha_{12} = 9.28491 \tag{62}$$

To sum up, for small x/k:

$$c^i(x,-1) \approx c^i_{(0)}(x,-1) \text{ of Eq. (61)} + \beta c^i_{(1)}(x,-1) \text{ of Eq. (62)} \tag{63}$$

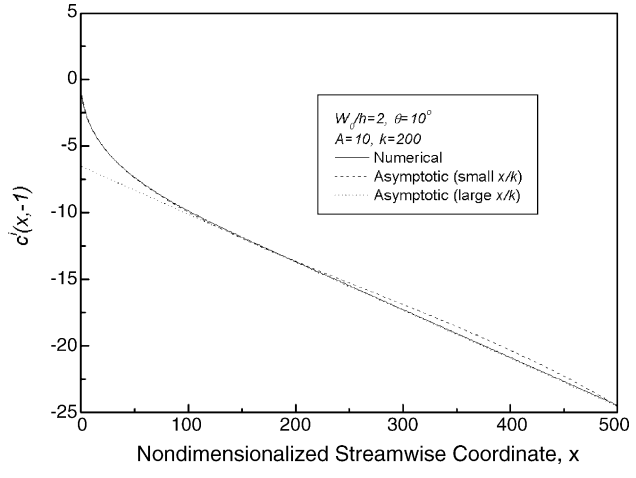

Fig. 12. Comparison of the asymptotic approximation derived in Section 4 with the numerical result ($A = 10$, $k = 200$, $\theta = 10^\circ$).

4.3. Comparison of asymptotic solutions with the numerical result

Fig. 12 presents the numerical result, together with asymptotic solutions for two limits of x/k. Eqs. (60) and (63) are in good agreement with the numerical result for nearly all ranges of x. In most regions, except at the start of channel, the large x/k condition can be applied, which produces the following formula for the change in concentration of species i:

$$c^i(x,-1) \approx -A\left[0.722\left(\frac{x}{k}\right) + 0.730\frac{W_0/h + 0.5526\tan\theta}{W_0/h + 2\tan\theta}\right] \tag{64}$$

5. Conclusion

A two-dimensional model was developed to imitate channel flow in a fuel cell. The effect of the inlet conditions and the channel geometry on the concentration distribution was investigated in the case of wall suction or injection. The product of the Reynolds number and the Schmidt number, k, was useful in manipulating the concentration distribution within the channel. For $k > 300$, the upper part of the channel was hardly affected by the reaction at the bottom. The draft angle of the channel was shown to suppress the change in concentration at the reaction site. The performance of the fuel cell for different values of the draft angle requires further study, together with the water-exhausting capability of a non-rectangular channel. For different limits of x/k, two asymptotic solutions were found that showed good agreement with the numerical result.

References

[1] S.M. Cox, A.C. King, Proc. R. Soc. Lond. A 453 (1997) 711.
[2] A.A. Kulikovsky, Electrochem. Commun. 3 (2001) 572.
[3] J. Larminie, A. Dicks, Fuel Cell Systems Explained, second ed., Wiley, 2003.
[4] R.J. Kee, M.E. Coltrin, P. Glarborg, Chemically Reacting Flow, Wiley, 2003.
[5] A.Z. Weber, J. Newman, J. Electrochem. Soc. 151 (2004) A326.
[6] S.J. Farlow, Partial Differential Equations for Scientists and Engineers, Dover Publications, New York, 1993.
[7] M.V. Dyke, Perturbation Methods in Fluid Mechanics, Parabolic Press, Stanford, CA, 1975.
[8] H. Stehfest, Commun. ACM 13 (1970) 47.
[9] H. Stehfest, Commun. ACM 13 (1970) 624.
[10] A. Davies, D. Crann, Int. J. Math. Educ. Sci. Technol. 30 (1999) 65.
[11] A.H.-D. Cheng, P. Sidauruk, Y. Abousleiman, Math. J. 4 (1994) 76.
[12] R.B. Bird, W.E. Stewart, E.N. Lightfoot, Transport Phenomena, second ed., Wiley, 2002.
[13] J.J. Baschunk, X. Li, J. Power Sources 86 (2000) 181.
[14] W. He, J.S. Yi, T.V. Nguyen, AIChE J. 46 (2000) 2053.
[15] G.J.M. Janssen, J. Electrochem. Soc. 148 (2001) A1313.
[16] U. Pasaogullari, C.Y. Wang, J. Electrochem. Soc. 151 (2004) A399.
[17] A.Z. Weber, R.M. Darling, J. Newman, J. Electrochem. Soc. 151 (2004) A1715.